Journal of
*Composites Science*

MDPI

*Article*

# Engineered GO-Silk Fibroin-Based Hydrogel for the Promotion of Collagen Synthesis in Full-Thickness Skin Defect

**Valeriia Syromiatnikova [1,†], Sharda Gupta [2,†], Margarita Zhuravleva [1], Galina Masgutova [1], Elena Zakirova [1], Alexander Aimaletdinov [1], Albert Rizvanov [1], Ilnur Salafutdinov [1,3], Ekaterina Naumenko [1,*] and Arindam Bit [2,*]**

1 Institute of Fundamental Medicine and Biology, Kazan Federal University, 420008 Kazan, Russia
2 Department of Biomedical Engineering, National Institute of Technology, Raipur 492001, India
3 Department of Medical Biology and Genetics, Kazan State Medical University, 420012 Kazan, Russia
* Correspondence: ekaterina.naumenko@gmail.com (E.N.); arinbit.bme@nitrr.ac.in (A.B.)
† These authors contributed equally to this work.

**Abstract:** In order to improve the regeneration of full-layer skin defects, hydrogels were developed based on the combination of chitosan (Cs), Daba silk fibroin (DSF), and graphene oxide (GO): CS, DSF/Cs and DSF/Cs/GO. The biocompatibility of hydrogels with human dermis fibroblasts in vitro was evaluated using the MTS assay. To assess the regenerative potential of hydrogels, a model of a full-layer skin defect was reconstructed on the back of rats and closed the wound surface with CS, DSF/Cs and DSF/Cs/GO hydrogels. The morphological and morphometric characteristics of regenerate tissues were obtained by staining with hematoxylin-eosin, Heidengain azocarmine, and immunohistochemistry on days 7 and 14 of the experiment. It has been shown that the use of DSF/Cs and DSF/Cs/GO promotes enhanced healing and epithelization of a full-layer skin wound. The addition of GO to the hydrogel increased the synthetic activity of fibroblasts and improved the characteristics of the produced collagen fibers.

**Keywords:** hydrogel; chitosan; silk fibroin; graphene oxide; skin wounds



**Citation:** Syromiatnikova, V.; Gupta, S.; Zhuravleva, M.; Masgutova, G.; Zakirova, E.; Aimaletdinov, A.; Rizvanov, A.; Salafutdinov, I.; Naumenko, E.; Bit, A. Engineered GO-Silk Fibroin-Based Hydrogel for the Promotion of Collagen Synthesis in Full-Thickness Skin Defect. *J. Compos. Sci.* **2023**, *7*, 186. https://doi.org/10.3390/jcs7050186

Academic Editor: Francesco Tornabene

Received: 3 March 2023
Revised: 24 April 2023
Accepted: 1 May 2023
Published: 5 May 2023



## 1. Introduction

Wound healing is a natural process that includes a cascade of complex cellular and biomolecular events that restore damaged wound tissue to its original state when an injury occurs. This process includes three different and overlapping phases: inflammation, cell proliferation (which includes neo-angiogenesis, granulation tissue formation, and re-epithelization), and the remodeling phase (i.e., neoangiogenesis extracellular matrix remodeling) [1]. If the injury violates the epidermis and dermis, wound healing is characterized by a fibrous regenerative process, which leads to the loss of all skin appendages and the formation of a scar [2]. The wounds heal due to marginal epithelization [3]; therefore, extensive full-thickness wounds cannot heal on their own, which leads to the formation of chronic wounds. Such wounds are not only a cosmetic defect, but a gateway to chronic infection and protein loss, which exhaust the patient, and is a cause of lifelong disability and serious public health problems [4].

Wound dressings have been used for ages to reduce pain, protect the wound and maintain a moist wound environment [5]. A dry gauze dressing is still the most commonly used material for primary dressing, but, it has multiple disadvantages—it does not support wet conditions, weakly absorbs exudate, and can also damage regenerate and cause pain when it is removed from the wound due to its adherence characteristics [6]. However, numerous studies had focused on the development of wet dressings, including hydrogel dressings designed to hold moisture on the surface of the wound, providing an ideal environment for wound cleaning and regeneration [7].

Chitosan is a cationic polymer obtained by the N-deacetylation of chitin, which has attracted great attention as a biomedical material. Chitosan hydrogels are widely used in the engineering of bone, skin, and cartilage, since their ingredients resemble the components of tissue extracellular matrix [8]. Chitosan hydrogels demonstrate good effects in wound healing, hemostatic properties, antimicrobial activity [9], anti-inflammatory properties, biocompatibility, and biodegradability [10]. Polysaccharide-based hydrogels have excellent biocompatible and biodegradable properties. Mengying Zhang et al. presented an efficient method for making macroporous polysaccharide hydrogels composed of dextran and polydopamine for the controlled release of antibiotics, which showed good antibacterial and wound healing properties [11]. In another work, Xianqin Tong et al. used another polysaccharide, curdlan, and polydopamine, to create a composite hydrogel for periodontal treatment, combining photothermal and antimicrobial effects at the same time [12] from laboratories to clinics.

Another natural polymer with a number of properties useful in regenerative medicine is silk fibroin, a natural protein obtained from the domestic silkworm Antheraea mylitta (A. mylitta). It is biocompatible, biodegradable, and has remarkable mechanical strength, low immunogenicity, gas permeability, hemostatic and anti-inflammatory properties [13]. In addition, one of the important physical properties is the formation of gels that can be easily attached to the skin independent of biological adhesives [14]. Silk fibroin nanofibers have been reported to promote the integration of human keratinocytes and fibroblasts and also enhance the deposition of type I collagen in vitro [15].

Graphene is one of the crystalline forms of carbon, which is a sp2 monolayer of hybridized orbitals in a densely packed two-dimensional (2D) honeycomb lattice, which has unusual mechanical, thermal, electronic properties, and remarkable biocompatibility [16]. Among graphene derivatives, graphene oxide (GO) has shown great promise for tissue regeneration, particularly in skin regeneration due to its high surface area to protein adsorption properties. It has been previously demonstrated that GO-poly (lactic-co-glycolic acid)/collagen (GO-PLGA/collagen) hybrid fiber sheets can promote the adhesion of dermal skin fibroblasts, showing its potential in repairing skin defects [17].

In the current study, chitosan, silk fibroin, and graphene oxide were combined with their potential to stimulate skin regeneration. Thereby, a new type of combined hydrogel dressings was created, and its effect on the regeneration of a full-layer skin defect was evaluatedat in-vivo.

Interpretation of the results of the histological examination is often subjective and does not allow for a comparative quantitative analysis. In this study, we tried to create a convenient protocol for the quantitative assessment of the scar morphological characteristics, based on a routine staining technique (Heidengain azocarmine) and digital image analysis in widespread software (ImageJ, Version 1.53t). The following characteristics of the regenerated tissue were analyzed: the size of the residual non-epithelialized defect, the thickness of the epidermis in the central part of the defect on the 14th day after the surgery, vascularization, the density of collagen bundles in the scar, their thickness, coherency and maturity of collagen.

There is no doubt that angiogenesis plays a key role in all phases of skin regeneration. Vessels promote leucocyte migration and cell debris elimination during the inflammation phase, supply regenerates with oxygen and nutrients to support cell proliferation, and also take part in the remodeling process providing cytokines, enzymes and cell migration [17]. At the same time, there is evidence in the literature, that pathological scar tissue is characterized by excessive vascularization. During the initial stages of healing, rich vascularization contributes to better regeneration, however, as the proliferative process slows down, vascularization normally decreases. The persistence of high vascularization in the remodeling phase is a characteristic of hypertrophic or keloid scar formation [18].

Another important characteristic of the scar is its collagen fibers morphology. During collagen maturation, the fiber diameter reflects the collagen maturity stage: thin collagen fibrils of 30–300 nm come together and form 1–20-micron thick fibers [19]. In healthy

skin, collagen bundles are organized randomly, whereas in the scar orientation, it is more parallel [20]. Clemons et al. (2018) suggested coherency analysis in the OrientationJ plugin of ImageJ to study fiber orientation. Randomly oriented fibers correspond to minimal coherency. The more the angular deviation differs from 90°, the higher is coherency [21]. Another quantitative characteristic of the healing process is the accumulation of collagen, which can be determined by the area of specifically stained collagen fibers in the section. It is predicted that over time, after the formation of the defect, the amount of collagen will increase, reflecting the dynamics of healing and the intensity of synthetic processes in the wound [22]. However, comparing the density of collagen fibers in the scar and intact tissue, it should be noted that fibers in the scar are predominantly parallel and packed more densely [23]. According to this Ukong et al. (2008) suggested one more method of collagen maturity assessment in ImageJ RBG color histogram mode using a blue:green ratio as the comparison criteria [24].

The above-mentioned methods of morphometric assessment were used in the current study to obtain reliable quantitative results. The described complex algorithm has the prospect of application for a comprehensive assessment of scar tissue in various studies.

## 2. Materials and Methods

### *2.1. Extraction of Silk Fibroin from Non-Mulberry Cocoon*

Daba cocoons were acquired from Chhattisgarh Khadi Gram Udyog, Chhattisgarh, India. Non-mulberry tussar cocoon of Daba ecorace was cut into small pieces and boiled in an aqueous solution of 0.2 M $NaHCO_3$ (Loba Chemie, Mumbai, India) at 90 °C for 1 h. The degummed silk fibers were rinsed thrice with ultrapure water to remove the gum-like sericin protein. The degummed fiber to solvent ratio will be maintained at 11 gm/100 mL. The fibers were then dissolved in calcium nitrate tetrahydrate at 80 °C until it was dissolved. The obtained viscous solution was dialyzed against polyethylene glycol (10 *w*/*v*%) (Sigma Aldrich, St. Louis, MI, USA) using a dialysis membrane (LA393, MWCO 12–14 kDa, Himedia, Thane, India) for 72 h to obtain high molecular weight silk fibroin [25]. Once it is dialyzed, the fibroin solution was centrifuged, to remove debris and silk aggregates. The concentration of the prepared silk fibroin solution was calculated using gravimetric analysis. The final silk fibroin solution in an aqueous silk fibroin solution was approximately 8% (*w*/*v*). The porous silk fibroin material was made by vacuum freeze drying the silk fibroin solution for 22 h, followed by heat treatment at 70 degree centigrade for 4 h.

### *2.2. Hydrogels Production*

Silk fibroin porous material was dissolved in milliQ water to obtain silk fibroin solution used for preparing hydrogels immediately before application. An aqueous 2% (*w*/*v*) Chitosan (Sigma, USA (417963)) stock solution was prepared by dissolving chitosan powder in an aqueous acetic acid solution (1% (*v*/*v*)). To prepare Cs hydrogel, 1000 µL genipin solution was added to the chitosan stock solution. As well, a stock solution of (0.01%) graphene oxide (GO) was prepared by dissolving GO powder in distilled water followed by ultrasonication for 60 min to obtain a uniform dispersion of GO throughout the solution. The modified Hummer technique was used to prepare GO powder [25]. The blend of chitosan solution and silk fibroin solution was sonicated for 5 min to obtain white-colored DSF/Cs (1:0.8) hydrogel. With the addition of graphene oxide solution, the viscosity of the chitosan-silk solution increased. The solution of DSF/CS/GO (1:0.8:0.02) mixture was shaken using a vortex mixer to form DSF/CS/GO hydrogel. The GO was added in low concentration to avoid aggregation of GO.

### *2.3. MTS Assay*

The analysis of the cytotoxicity of hydrogels in-vitro was carried out using a culture of human skin fibroblast cells of the 4th passage. Skin fibroblasts were obtained by explant method from a skin sample of a healthy volunteer with informed consent during routine

abdominoplasty. Cells were seeded in four replications for each experimental group on a 96-well plate pre-coated with hydrogels DSF/Cs or DSF/Cs/GO or Cs in a volume of 50 µL per well, 10,000 cells per well in 200 µL of aMEM + 10% FBS medium (PanEco, Moscow, Russia) and cultured in a humidified 5% $CO_2$ atmosphere at 37 °C. MTS test was performed at two time-points: one hour and 24 h. For the MTS test, MTS (Sigma, USA) and PMS (Diam, Moscow, Russia) reagents were mixed in a ratio of 20:1 and 20 µL of a mixture of reagents were added per well, incubated for 1 h in a humidified 5% $CO_2$ atmosphere at 37 °C before the optical density of supernatants of the samples was evaluated on a microplate reader Infinite M200Pro (Tecan, Männedorf, Switzerland) in the two-wave mode: main filter—490 nm, reference filter—640 nm.

### *2.4. In Vivo Studies*

Full-layer skin defect formation was made on the back of rats. Experiments were performed using 32 white male Wistar rats aged 6–8 weeks each, weighing 200–300 g (GMBH «Nursery RAMTN», Moscow, Russia). Animals were kept under standard vivarium conditions in the day/night mode 12/12 with free access to food and water.

The procedure for the formation of a full-layer skin defect had been developed. The experiment was performed in four replications for each observation period. For anesthesia, a 6.4% solution of chloral hydrate (Dia-M, Russia) was used at the rate of 400 mg of dry matter per 1 kg of animal weight. Hairs were removed with a depilatory cream. The skin was treated with a 70% ethanol solution. A full-layer around 1 cm in diameter skin defect was formed on the back with surgical scissors [26]. Hydrogels were applied in a volume of 300 µL per wound. The controls were wounds with hydrogel based on Cs only and wounds without any hydrogel. The wounds were closed with a fabric-based plaster to isolate the wound, and the dressing was changed on day 3 followed by alternative day. The animals were sacrificed on days 7 and 14 of the experiment, the tissues of the wound were taken for histological examination. The total period of observation of wounds was 14 days, which was due to the dynamics of the wound-healing process.

### *2.5. Histology Procedure*

To take histological specimens, animals were anesthetized as described in the previous section. They were perfused transcranial with a pre-chilled PBS (pH 7.4), then, with pre-chilled 10% buffered formalin. Areas of skin defects were isolated with adjacent intact tissues and underlying muscles. Samples were fixed in 10% buffered formalin, dehydrated in ethanol solutions of increasing concentrations, and embedded in paraffin (BioVitrum, Saint Petersburg, Russia). Paraffin tissue sections of 5 µm thick were made on an HM 355S rotary microtome (Thermo Scientific, Waltham, MA, USA). Hematoxylin and eosin staining were used to give a general morphological characteristic to determine leukocyte infiltration. To assess the synthesis of collagen, the Heidengain azocarmine (BioVitrum, Russia) stain was used. To count vascularization and for determining the size of the non-epithelialized defect, immunohistochemical staining with antibodies to CD31 (abcam, ab182981) and pancytokeratin (BioLegend, San Diego, CA, USA, 914204), respectively, were used. Novolink Polymer Detection System was used to visualize immune precipitate (Leica, Wetzlar, Germany, RE7150-K). Microphotographs were taken using Aperio ImageScope 12.1 (Leica). The size of the residual defect, the thickness of the epidermis, vascularization, and collagen fibers thickness were evaluated in ImageScope software (Leica). The density of collagen fibers was estimated by the area occupied by collagen fibers (area measurement) in ImageJ (Wayne Rasband, National Institutes of Health) [22]. Coherency analysis was performed in the OrientationJ plugin of ImageJ [21]. Collagen blue: green ratio was measured using an ImageJ RBG color histogram [24].

### 2.6. Statistical Analysis

Statistical analysis was performed using SPSS Statistics 17.0 Software (SPSS, Chicago, IL, USA) and RTCA Software (Version 1.2). The values were represented as mean ± standard deviation (SD). One-way analysis of variance (ANOVA) with Tukey's test was used to evaluate statistical significance with $p$-value < 0.05.

## 3. Results

### 3.1. Confirmation of GO

For the confirmation of the preparation of Graphene oxide, XRD was performed and it was found that a wide peak was found at 2θ = 11.6°. This indicates the successful preparation of graphene oxide as shown in Figure 1.

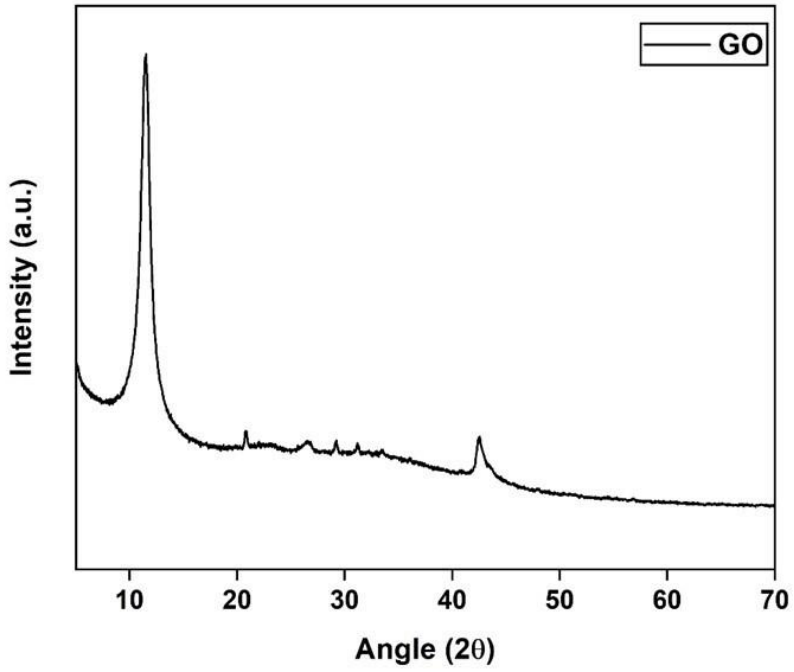


**Figure 1.** XRD spectra of graphene oxide showing a peak at 2θ = 11.6° confirming successful preparation of graphene oxide.

### 3.2. In Vitro Studies

Morphology of human skin fibroblast cells was analyzed during cultivation under hydrogels coverage. It was demonstrated that one hour after the coating with gels, the cells became rounded, and partially detached from the dish. After 24 h of cultivation under the DSF/Cs/GO gel, the cells had normal fibroblast-like morphology, while in the DSF/Cs and Cs groups had a significant part of the cells detached, and cells with normal morphology were found only on the periphery of the wells (Figure 2A).

In vitro analysis of hydrogels cytotoxicity for human dermal fibroblasts cell culture had shown that both variants of the DSF/Cs and DSF/Cs/GO hydrogels had supported the proliferation of skin fibroblasts. However, a significant decrease in the activity of mitochondrial dehydrogenases was observed compared with the control group of human skin fibroblasts. The lowest cell proliferation was detected on pure Cs hydrogel (Figure 2B).

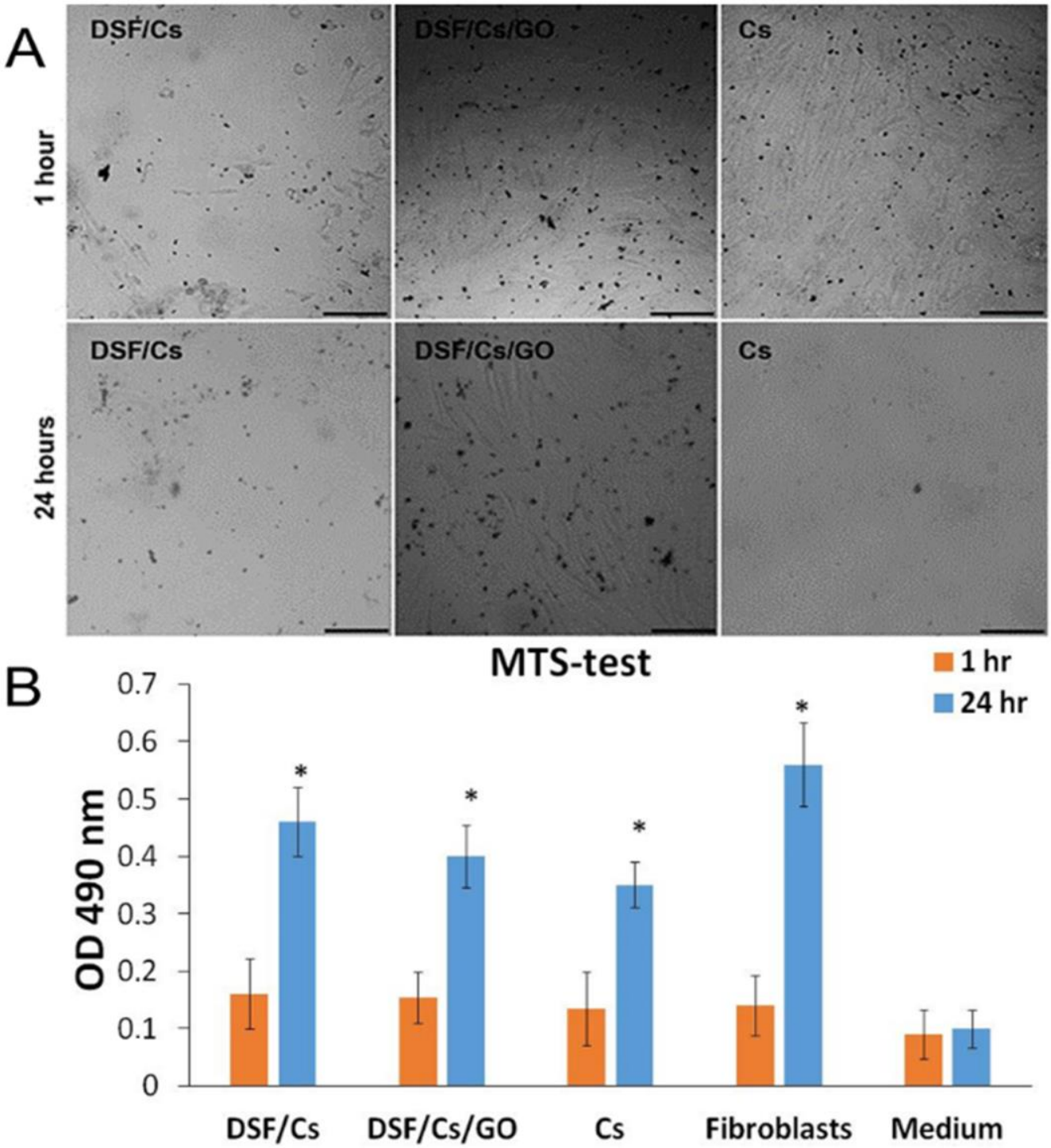


**Figure 2.** The analysis of the cytotoxicity of hydrogels in vitro. (**A**)—morphology of fibroblasts grown on different types of hydrogels, scale bar 100 μm. (**B**)—MTS-test results of fibroblast cells incubated in prepared hydrogel for one and 24 h. * $p < 0.05$.

### 3.3. In Vivo Studies

For comparison of wound healing efficiency of the prepared hydrogels, histological evaluation of the repaired tissue with Hematoxylin-eosin (Figure 3) and Heidenhain azocarmine staining (Figure 4) was conducted on day 7 and day 14.

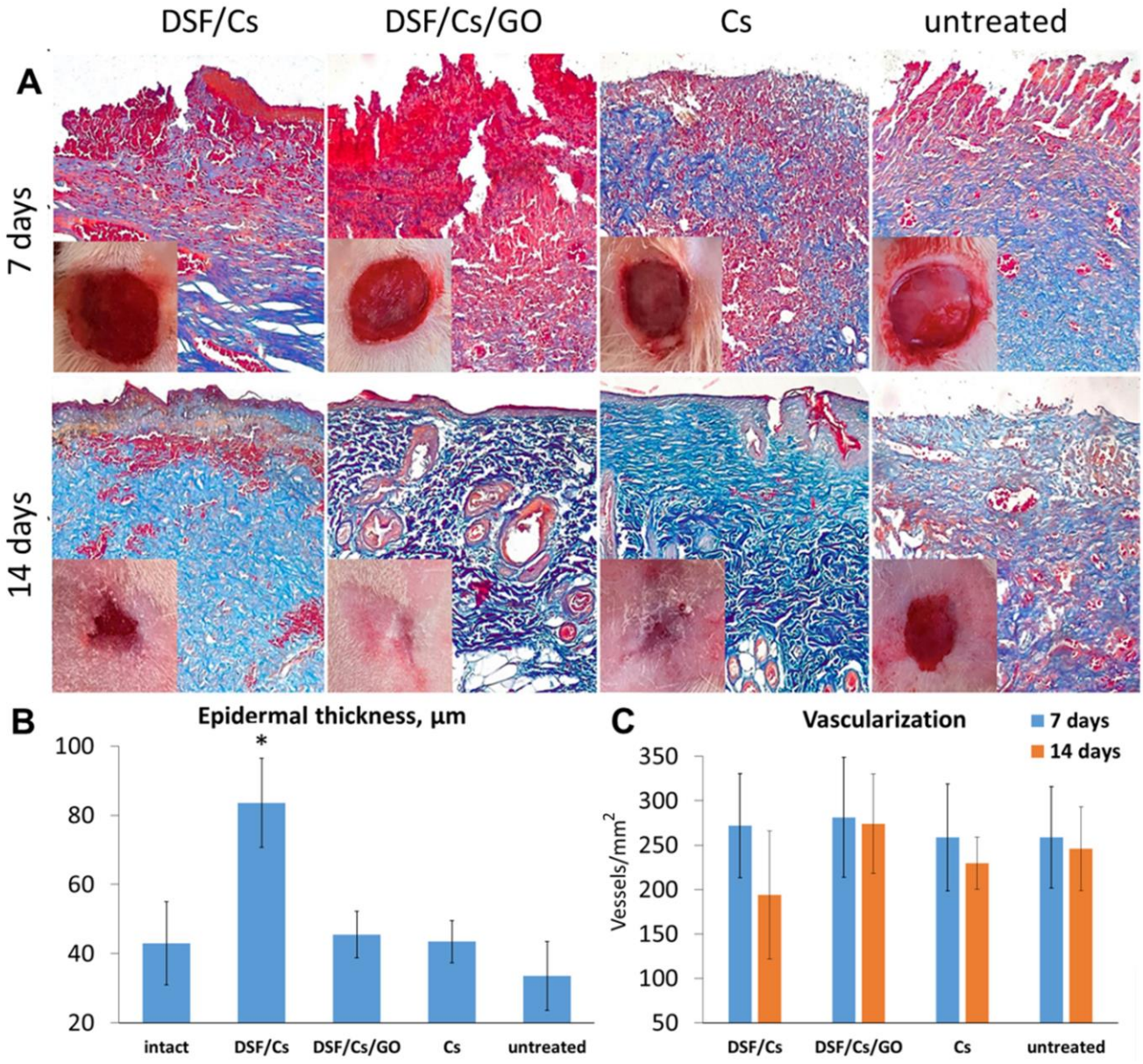


**Figure 3.** State of wounds on 7 and 14 days after the formation of full-layer skin defect. (**A**)—the general appearance of wounds and Hematoxylin eosin, ×100. (**B**)—Morphometric analysis of regenerates: thickness of epidermis in the central part of wounds on the 14th day after surgery; (**C**)—vascularization regenerates. * $p < 0.05$.

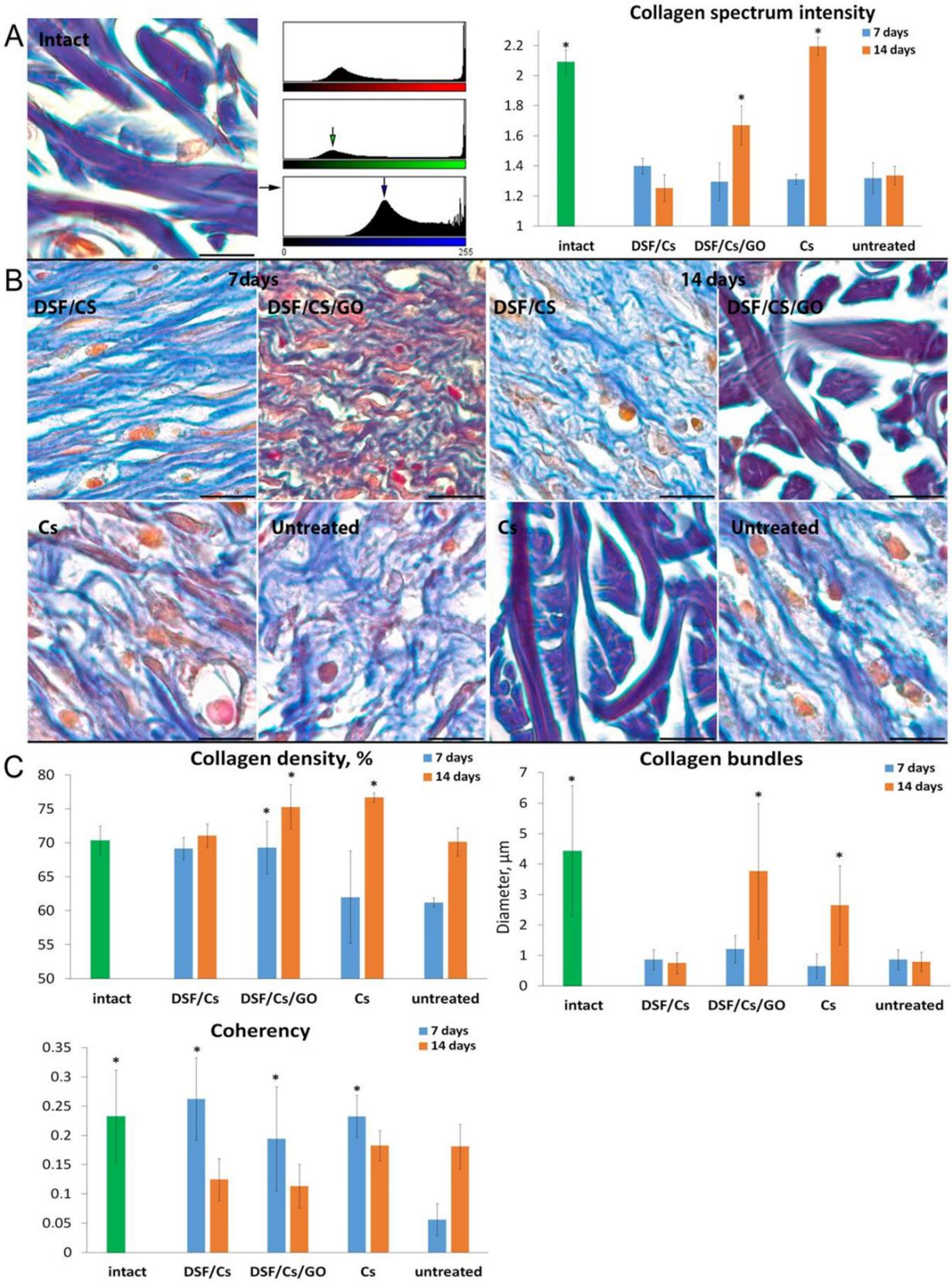


**Figure 4.** Histomorphometry of collagen bundles in full-layer skin wounds on 7 and 14 days after the formation of the defect. (**A**)—Collagen spectrum intensity analysis. (**B**)—Scar tissue. Heidenhain azocarmine staining. Scale bar 100 µm. (**C**)—Histomorphometry of collagen fibers. * $p < 0.05$.

In the case of DSF/CS hydrogel, on the 7th day after the skin defect formation, the wound was moist, areas of local inflammation were observed. The area of gel application was richly infiltrated with leucocytes. Extensive microhemorrhages were also observed. The tissue under the crust contained parallel thin bundles of collagen fibers of light blue color with a diameter of 0.86 ± 0.33 μm. The collagen spectrum corresponded to immature collagen, and they did not differ from the spectrum of fibers in an untreated defect, or a defect filled with Cs gel (Figure 4A). The coherence of the direction of collagen fibers was significantly higher than in the untreated defect (Figure 4C). Vascularization was 311.34 ± 58.6 vessels/mm$^2$, which did not significantly differ from control samples (Figure 3C). The regenerated tissue was significantly denser than untreated samples, or when Cs gel was applied. Marginal epithelization was also observed. The diameter of the residual non-epithelialized defect was 1257–3234 μm. No cases of complete epithelization were observed in this group. On the 14th day after the operation, the residual defect was up to 2137 μm, and the wound was moist. Cases of complete epithelization were also observed. The regenerated epidermis had a thickness of 83.6 ± 12.9 μm (Figure 3B) and was composed of 6.9 ± 1.3 layers, which was significantly higher than in the untreated defect (thickness 33.6 ± 10 μm, 2.5 ± 0.7 layers of cells). The underlying area (as on the 7th day), contained microhemorrhages, although vascularization had decreased to 194 ± 72.2 vessels/mm$^2$ (Figure 3C). Bundles of collagen fibers were thin 0.75 ± 0.34 μm. Collagen fibers were predominantly disordered, the coherence had decreased in comparison with samples taken on the 7th day, and it was lower than that in an untreated defect or defect covered by Cs gel. Fibers were stained light blue with aniline blue, which corresponded to the spectrum of immature collagen. Collagen fibers were localized as dense as in the intact skin. The obtained data indicated the formation of normal scar tissue in the area of the defect.

In the case of DSF/Cs/GO hydrogel, on the 7th day after the formation of the full-layer skin defect, the wound defect was moist with a large amount of residual gel. The central part of the wound was containing a well-vascularized (271.72 ± 67.62 vessels/mm$^2$) (Figure 3C) granulation tissue. Thin bundles of parallel collagen fibers of 1.21 ± 0.45 μm thick were penetrating the gel residues. The coherence of the direction of collagen fibers was significantly higher in a treated wound than in an untreated wound. Collagen fibers were stained light blue with aniline blue for identifying the spectrum of immature collagen. Collagen fibers were found much denser than in the control or the Cs group. Granulation tissue at the bottom of the wound was moderately infiltrated with leukocytes, a small number of microhemorrhages, and few vessels with erythrostasis. Erythrocyte diapedesis was also observed. Both cases of marginal epithelization and complete epithelization were observed under the crust. The size of the residual non-epithelialized defect was 0–5034 μm. On the 14th day after the surgery, complete epithelized scar formation was observed. A thin layer of keratinocytes was also observed, located in 4 ± 1st rows, with a thickness of 45.5 ± 6.8 μm, and it was not significantly varying from the parameters of the untreated defect. The underlying connective tissue contained glands and hair follicles; whereas, thick strands of disordered collagen fibers were stained intense blue. Analyzing the coherence of the direction of collagen fibers, it was found that the fibers were predominantly disordered. The coherence had decreased with the healing period on the 7th day, and was lower than the control group. The fibers stained intense blue with aniline blue, the spectrum of which corresponded to mature collagen, and it was significantly different from the results obtained on day 7 and day 14 in an untreated defect (Figure 4B). The density of collagen fibers did not differ from that in the intact skin. The thickness of the bundles of collagen fibers had increased significantly compared with that on the 7th day and it had reached 3.77 ± 2.21 μm, which was also significantly higher than in the untreated defect (Figure 4C). Closure of the wound due to contraction was most pronounced in this group. The data indicated an almost complete restoration of the skin in the damaged area. The characteristics of the regenerated tissue were closer to the properties of the intact dermis.

In the case of Cs hydrogel, on the 7th day after the surgery, the wound was hydrated, with smooth edges. The surface of the wound was represented by granulation tissue, with thin disordered bundles of collagen fibers stained in light blue. The thickness of collagen fibers was 0.65 ± 0.4 μm, and their spectrum corresponded to immature collagen. The coherence of the fiber direction was relatively high, similar to that of the intact dermis. The fibers were significantly strangled compared to samples treated with DSF/Cs or DSF/Cs/GO gels. The fiber coherency was significantly higher than that of the untreated defect. The tissue was richly vascularized (281.3 ± 60.2 vessels/mm$^2$) (Figure 3C), with moderate leucocyte infiltration. Marginal epithelization was also observed. On the 14th day after the formation of the skin defect, complete wound epithelization with a thin layer of keratinocytes (3–4 layers 43.5 ± 6.1 μm thick) (Figure 3B) was observed. The epidermis became thinner in the central part of the scar. The connective tissue under the central part of the scar contained a layer of densely parallel thin collagen fibers stained with light blue, covering a layer of mature collagen with thicker fibers (2.65 ± 1.3 μm). This underlying layer was stained intensely with blue and contained glands and hair follicles. Collagen fibers were denser than in an untreated defect, intact dermis, or after DSF/Cs treatment. The coherence of collagen fibers was higher than post-DSF/Cs or post-DSF/Cs/GO gel treatment, and did not differ from that in the untreated defect. Vascularization had decreased slightly—(229.6 ± 29.15 vessels/mm$^2$) (Figure 3C). Epidermis bordering the scar was significantly thickened. The obtained data indicated the formation of dense rough scars in Cs treated group due to enhanced connective tissue formulation.

In the case of untreated control, on the 7th day after the formation of the full-layer skin defect, the wound was moist, while the absence of gel had confirmed the formation of dense connective tissue bordering the wound edges. This formation was easily separated with a slight tension of the edges of the wound. Thus, in case of violation of the newly formed connective tissue, by day 14, an unepithelized wound surface was observed, while maintaining tissue as an epithelized scar. On the 7th day, this formation was represented by connective tissue with thin (0.86 ± 0.33 μm) (Figure 4C) bundles of collagen fibers stained in light blue, and was coated with granulation of tissue. The tissue got moderately vascularized (281.34 ± 60.25 μm) (Figure 3C), and was superficially infiltrated with leucocytes. There was marginal epithelization, and the diameter of the residual defect was 2390 ± 924 μm). After 14 days, complete wound epithelization was observed with a thin layer of the epidermis in 2.5 ± 0.71 layers, with a thickness of 33.6 ± 10 μm on newly formed connective tissue. The underlying connective tissue was represented by mature collagen fibers, stained intensely blue, containing glands and hair follicles. Vascularization was formed at a density of 246.17 ± 47.15 vessels/mm$^2$ (Figure 3C). By day 14, the wound had contracted to a diameter of 5567 μm. The surface layers of the wound had shown signs of hypotrophic scar formation with thin and sparse collagen fibers, and stained pale. The formation of scar tissue in this group was slower than in gel-treated groups.

## 4. Discussion

The goal of this study was to evaluate the effectiveness of hydrogels based on chitosan, Daba silk fibroin, and graphene oxide for the regeneration of full-layer skin defects. According to numerous previous studies, each of the components of the developed hydrogels had individually promoted the healing of skin wounds [27]. Hence, a combined form of all components was made to formulate the hydrogels to achieve a more pronounced, and synergistic effect in regenerated skin.

The results of the MTS test had shown that the hydrogels DSF/Cs and DSF/Cs/GO supported the proliferation of skin fibroblasts in vitro, and their proliferation on these gels was higher than on pure Cs hydrogel. Thus, this effect was due to direct exposure to DSF. The obtained data correlates with the results of other researchers, who had shown that silk fibroin had promoted the adhesion and proliferation of dermal fibroblasts [28]. The activity of mitochondrial dehydrogenases of cells seeded on hydrogels was lower as compared to a control culture that did not contain any gels. This effect might be due to the fact that

cell cultures were more sensitive to external influences or fluctuations in the chemical composition of the medium than cells in tissues in vivo. Nevertheless, an important research result is the principal in vitro biocompatibility of the developed hydrogels, and the possibility of proliferation and survival of dermal fibroblasts in their presence.

Marginal migration and proliferation of fibroblasts, followed by the formation of an extracellular matrix, are key factors in the formation of granular tissue [29]. In this study, scars in all groups had a trend to be normotrophic. Thicker and more mature collagen fibers were observed on day 14 using DSF/Cs/GO hydrogel and pure Cs, but the fiber density was higher with the DSF/Cs hydrogel composition. A similar effect was observed in the work of Movaffagh J. et al. (2019) who reported an increase in collagen production leading to accelerated wound healing when using chitosan-containing multilayer hydrogel dressings applied to full-layer wounds in diabetic rats [9]. However, when DSF was added to Cs, the fiber thickness decreased, and when GO was added, this effect was leveled. The production of thick collagen bundles in the Cs group could be associated with its mild local irritating effect [30], which had decreased in DSF/Cs group due to the dilution with DSF. Collagen was promoting fibroblasts, and it had been observed that fibroblasts proliferate and were better and had retained their morphology in gels with the addition of GO. These data correlate with the study [31] which had shown GO biocompatibility with fibroblasts, and increased activity of mitochondrial dehydrogenases in fibroblast cells under its action. Lasocka et al. (2019) reported that this effect might be due to the contact of fibroblasts with a rough GO surface, which had caused intracellular mechanical stress, providing a complex of signals, leading to increased local adhesion and cell stimulation to migration and proliferation, which ultimately alters their synthetic activity [32]. On the other hand, when DSF was added to Cs, it slightly decreased the viscosity of the resulting gel, which might be the reason for the decrease in the adhesion of fibroblasts with a subsequent decrease in their collagen synthetic activity.

Another part of the wound healing mechanism is contraction, whose contribution to the defect closure is great in rodents [33]. In DSF/Cs/GO group, this contraction was most pronounced, which led to the best morphological characteristics of the formed scar. This effect can be associated with GO addition, which significantly affects the myoblasts' cellular behavior. The surface topography of extracellular GO, and its roughness can provide mechanical signaling which can stimulate muscle progenitor cells [34]. Moreover, it was previously shown that GO combined with chitosan could induce spontaneous differentiation of myoblasts [35].

When applying DSF/Cs and DSF/Cs/GO gels on the 7th day, the collagen fiber density was found higher than that of Cs gel and control groups. It indicates better stimulation of fibroblasts for the synthesis of an extracellular matrix under the influence of developed hydrogels. By the 14th day, this influence had disappeared, which may be due to the natural process of regeneration in the wound. Thus, the use of DSF/Cs and DSF/Cs/GO gels provides faster formation of connective tissue elements in the early stages after damage.

In our study, the use of DSF/Cs and DSF/Cs/GO hydrogels had shown a better effect in wound epithelialization, compared to an untreated defect and a defect covered with pure Cs hydrogel. These findings correlated with studies [36] which demonstrated that the silk fibroin scaffolds provide good structural support for the spread and attachment of keratinocytes.

Adequate blood supply is essential for proper regeneration of wounds. In all studied groups on the 7th day after the surgery, regenerated tissues were richly vascularized. Whereas, on the 14th day the vascularization had decreased, which is typical for the normal remodeling phase. We modified the composition of the gels by adding GO in order to enhance angiogenesis in the wound area, due to its pro-angiogenic effect [37]. Nevertheless, vascularization in the group with GO addition on the 14th day was found similar to that of other groups, so GO used in the study did not provide a significant effect on vascularization in the region of a full-layer skin defect. Enhanced vascularization in DSF/Cs/GO group did not lead to the formation of a hypertrophic scar. Probably, the addition of GO did

not have an effect due to the fact that wounds initially had good regenerative potential and vascularization was high. In a model of the ischemic wound, GO could have a better effect [38]. It was also previously shown that GO may have both pro-and anti-angiogenic potential depending on the concentration used [39].

## 5. Conclusions

In conclusion, the developed hydrogels had a positive effect on the regeneration of skin after the formation of the full-layer defect. The best morphological characteristics of the regenerated tissue were achieved using a hydrogel with GO addition, which was explained by its complex composition and synergistic action of the components. The digital methods used for processing tissue section microphotographs made it possible to carry out a quantitative comparative analysis of the effects of various hydrogel variants. An important promising result of applying the analysis technique is the ability to carry out a comparative analysis of the results of various experiments performed at different times.

**Author Contributions:** Conceptualization, A.B., I.S. and A.R.; methodology, I.S. and A.B.; formal analysis, S.G., I.S. and E.N.; investigation, V.S., S.G., M.Z., G.M., E.Z. and A.A.; data curation, E.N.; writing—original draft preparation, V.S., E.N. and I.S.; writing—review and editing, A.B., I.S. and A.R.; visualization, E.Z., V.S., M.Z. and G.M.; supervision, A.B. and I.S.; project administration, I.S. and A.R. All authors have read and agreed to the published version of the manuscript.

**Funding:** Work was funded by the Grant of Russian Foundation for Basic Research Ind-A 18-54-45023 "Investigation of fundamental mechanisms of regeneration of deep-layer skin wounds in response to treatment with polyelectrolyte-hydrogel complex dressings and gene therapy", Indo-Russian grant (INT/RUS/RFBR/P-332) and SERB Early Career Award (ECR/2017/001115) to Arindam Bit. Histoprocessing was funded by RSF according to the research project No. 23-25-00282.

**Data Availability Statement:** All data generated or analyzed during this study are included in this published article. The data that support the findings of this study are available from the corresponding author upon request.

**Acknowledgments:** This paper has been supported by the Kazan Federal University Strategic Academic Leadership Program (PRIORITY-2030).

**Conflicts of Interest:** The authors declare that the research was conducted in the absence of any commercial or financial relationships that could be construed as a potential conflict of interest.

## References

1. Gonzalez, A.; Costa, T.; Andrade, Z.; Medrado, A. Wound healing—A literature review. *An. Bras. De Dermat* **2016**, *91*, 614–620. [CrossRef]
2. Takeo, M.; Lee, W.; Ito, M. Wound healing and skin regeneration. *Cold Spring Harb. Perspect. Med.* **2015**, *5*, a023267. [CrossRef] [PubMed]
3. Sardari, K.; Kakhki, E.G.; Mohri, M. Evaluation of wound contraction and epithelialization after subcutaneous administration of Theranekron® in cows. *Comp. Clin. Pathol.* **2007**, *16*, 197–200. [CrossRef]
4. Molnar, J.A.; Underdown, M.J.; Clark, W.A. Nutrition and chronic wounds. *Adv. Wound Care* **2014**, *3*, 663–681. [CrossRef] [PubMed]
5. Jones, V.; Grey, J.E.; Harding, K.G. Wound dressings. *BMJ* **2006**, *332*, 777–780. [CrossRef] [PubMed]
6. Sood, A.; Granick, M.S.; Tomaselli, N.L. Wound dressings and comparative effectiveness data. *Adv. Wound Care* **2014**, *3*, 511–529. [CrossRef]
7. Kamoun, E.A.; Kenawy, E.-R.S.; Chen, X. A review on polymeric hydrogel membranes for wound dressing applications: PVA-based hydrogel dressings. *J. Adv. Res.* **2017**, *8*, 217–233. [CrossRef]
8. Demirtaş, T.T.; Irmak, G.; Gümüşderelioğlu, M. A bioprintable form of chitosan hydrogel for bone tissue engineering. *Biofabrication* **2017**, *9*, 035003. [CrossRef]
9. Movaffagh, J.; Bazzaz, F.; Yazdi, A.T.; Sajadi-Tabassi, A.; Azizzadeh, M.; Najafi, E.; Amiri, N.; Taghanaki, H.B.; Ebrahimzadeh, M.H.; Moradi, A. Wound Healing and Antimicrobial Effects of Chitosan-hydrogel/Honey Compounds in a Rat Full-thickness Wound Model. *Wounds Compend. Clin. Res. Pract.* **2019**, *31*, 228–235.
10. Yoon, S.-J.; Hyun, H.; Lee, D.-W.; Yang, D.H. Visible light-cured glycol chitosan hydrogel containing a beta-cyclodextrin-curcumin inclusion complex improves wound healing in vivo. *Molecules* **2017**, *22*, 1513. [CrossRef]

11. Zhang, M.; Huang, Y.; Pan, W.; Tong, X.; Zeng, Q.; Su, T.; Qi, X.; Shen, J. Polydopamine-incorporated dextran hydrogel drug carrier with tailorable structure for wound healing. *Carbohydr. Polym.* **2021**, *253*, 117213. [CrossRef] [PubMed]
12. Tong, X.; Qi, X.; Mao, R.; Pan, W.; Zhang, M.; Wu, X.; Chen, G.; Shen, J.; Deng, H.; Hu, R. Construction of functional curdlan hydrogels with bio-inspired polydopamine for synergistic periodontal antibacterial therapeutics. *Carbohydr. Polym.* **2020**, *245*, 116585. [CrossRef] [PubMed]
13. Baruah, R.R.; Kalita, M.C.; Devi, D. Novel non-mulberry silk fibroin nanoparticles with enhanced activity as potential candidate in nanocarrier mediated delivery system. *RSC Adv.* **2020**, *10*, 9070–9078. [CrossRef]
14. Im, D.S.; Kim, M.H.; Yoon, Y.I.; Park, W.H. Gelation behaviors and mechanism of silk fibroin according to the addition of nitrate salts. *Int. J. Mol. Sci.* **2016**, *17*, 1697. [CrossRef]
15. Min, B.-M.; Lee, G.; Kim, S.H.; Nam, Y.S.; Lee, T.S.; Park, W.H. Electrospinning of silk fibroin nanofibers and its effect on the adhesion and spreading of normal human keratinocytes and fibroblasts in vitro. *Biomaterials* **2004**, *25*, 1289–1297. [CrossRef]
16. Zhang, W.; Yin, B.; Xin, Y.; Li, L.; Ye, G.; Wang, J.; Shen, J.; Cui, X.; Yang, Q. Preparation, mechanical properties, and biocompatibility of graphene oxide-reinforced chitin monofilament absorbable surgical sutures. *Mar. Drugs* **2019**, *17*, 210. [CrossRef] [PubMed]
17. Wilgus, T.A.; Ferreira, A.M.; Oberyszyn, T.M.; Bergdall, V.K.; DiPietro, L.A. Regulation of scar formation by vascular endothelial growth factor. *Lab. Investig.* **2008**, *88*, 579–590. [CrossRef]
18. Amadeu, T.; Braune, A.; Mandarim-de-Lacerda, C.; Porto, L.C.; Desmoulière, A.; Costa, A. Vascularization pattern in hypertrophic scars and keloids: A stereological analysis. *Pathol.-Res. Pract.* **2003**, *199*, 469–473. [CrossRef]
19. Ushiki, T. The three-dimensional ultrastructure of the collagen fibers, reticular fibers and elastic fibers: A review. *Kaibogaku Zasshi. J. Anat.* **1992**, *67*, 186–199.
20. Van Zuijlen, P.P.; Ruurda, J.J.; Van Veen, H.A.; Van Marle, J.; Van Trier, A.J.; Groenevelt, F.; Kreis, R.W.; Middelkoop, E. Collagen morphology in human skin and scar tissue: No adaptations in response to mechanical loading at joints. *Burns* **2003**, *29*, 423–431. [CrossRef]
21. Clemons, T.; Bradshaw, M.; Toshniwal, P.; Chaudhari, N.; Stevenson, A.; Lynch, J.; Fear, M.; Wood, F.; Iyer, K.S. Coherency image analysis to quantify collagen architecture: Implications in scar assessment. *RSC Adv.* **2018**, *8*, 9661–9669. [CrossRef] [PubMed]
22. Caetano, G.F.; Fronza, M.; Leite, M.N.; Gomes, A.; Frade, M.A.C. Comparison of collagen content in skin wounds evaluated by biochemical assay and by computer-aided histomorphometric analysis. *Pharm. Biol.* **2016**, *54*, 2555–2559. [CrossRef] [PubMed]
23. Kim, J.Y.; Willard, J.J.; Supp, D.M.; Roy, S.; Gordillo, G.M.; Sen, C.K.; Powell, H.M. Burn scar biomechanics following pressure garment therapy. *Plast. Reconstr. Surg.* **2015**, *136*, 572. [CrossRef] [PubMed]
24. Ukong, S.; Ampawong, S.; Kengkoom, K. Collagen measurement and staining pattern of wound healing comparison with fixations and stains. *J. Microsc. Soc. Thail.* **2008**, *22*, 37–41.
25. Gupta, S.; Dutta, P.; Acharya, V.; Prasad, P.; Roy, A.; Bit, A. Accelerating skin barrier repair using novel bioactive magnesium-doped nanofibers of non-mulberry silk fibroin during wound healing. *J. Bioact. Compat. Polym.* **2022**, *37*, 38–52. [CrossRef]
26. Salafutdinov, I.I.; Gazizov, I.M.; Gatina, D.K.; Mullin, R.I.; Bogov, A.A.; Islamov, R.R.; Kiassov, A.P.; Masgutov, R.F.; Rizvanov, A.A. Influence of Recombinant Codon-Optimized Plasmid DNA Encoding VEGF and FGF2 on Co-Induction of Angiogenesis. *Cells* **2021**, *10*, 432. [CrossRef]
27. Gupta, S.; Prasad, P.; Roy, A.; Alam, M.M.; Ahmed, I.; Bit, A. Metallic ion-based graphene oxide functionalized silk fibroin-based dressing promotes wound healing via improved bactericidal outcomes and faster re-epithelization. *Biomed. Mater.* **2022**, *17*, 035010. [CrossRef]
28. Gholipourmalekabadi, M.; Sapru, S.; Samadikuchaksaraei, A.; Reis, R.L.; Kaplan, D.L.; Kundu, S.C. Silk fibroin for skin injury repair: Where do things stand? *Adv. Drug Deliv. Rev.* **2020**, *153*, 28–53. [CrossRef]
29. Spyrou, G.E.; Watt, D.; Naylor, I.L. The origin and mode of fibroblast migration and proliferation in granulation tissue. *Br. J. Plast. Surg.* **1998**, *51*, 455–461. [CrossRef]
30. Elnashar, M. *Biopolymers*; BoD–Books on Demand: Norderstedt, Germany, 2010.
31. Lasocka, I.; Szulc-Dąbrowska, L.; Skibniewski, M.; Skibniewska, E.; Strupinski, W.; Pasternak, I.; Kmieć, H.; Kowalczyk, P. Biocompatibility of pristine graphene monolayer: Scaffold for fibroblasts. *Toxicol. Vitr.* **2018**, *48*, 276–285. [CrossRef]
32. Lasocka, I.; Jastrzębska, E.; Szulc-Dąbrowska, L.; Skibniewski, M.; Pasternak, I.; Kalbacova, M.H.; Skibniewska, E.M. The effects of graphene and mesenchymal stem cells in cutaneous wound healing and their putative action mechanism. *Int. J. Nanomed.* **2019**, *14*, 2281. [CrossRef] [PubMed]
33. Sorg, H.; Tilkorn, D.J.; Hager, S.; Hauser, J.; Mirastschijski, U. Skin wound healing: An update on the current knowledge and concepts. *Eur. Surg. Res.* **2017**, *58*, 81–94. [CrossRef] [PubMed]
34. Bałaban, J.; Wierzbicki, M.; Zielińska, M.; Szczepaniak, J.; Sosnowska, M.; Daniluk, K.; Cysewski, D.; Koczoń, P.; Chwalibog, A.; Sawosz, E. Effects of graphene oxide nanofilm and chicken embryo muscle extract on muscle progenitor cell differentiation and contraction. *Molecules* **2020**, *25*, 1991. [CrossRef] [PubMed]
35. Lee, J.H.; Lee, Y.; Shin, Y.C.; Kim, M.J.; Park, J.H.; Hong, S.W.; Kim, B.; Oh, J.-W.; Park, K.D.; Han, D.-W. In situ forming gelatin/graphene oxide hydrogels for facilitated C2C12 myoblast differentiation. *Appl. Spectrosc. Rev.* **2016**, *51*, 527–539. [CrossRef]

36. Yu, P.; Guo, J.; Li, J.; Shi, X.; Wang, L.; Chen, W.; Mo, X. Repair of skin defects with electrospun collagen/chitosan and fibroin/chitosan compound nanofiber scaffolds compared with gauze dressing. *J. Biomater. Tissue Eng.* **2017**, *7*, 386–392. [CrossRef]
37. Mukherjee, S.; Sriram, P.; Barui, A.K.; Nethi, S.K.; Veeriah, V.; Chatterjee, S.; Suresh, K.I.; Patra, C.R. Graphene oxides show angiogenic properties. *Adv. Healthc. Mater.* **2015**, *4*, 1722–1732. [CrossRef]
38. Phelps, E.A.; Garcia, A.J. Update on therapeutic vascularization strategies. *Regen. Med.* **2009**, *4*, 65–80. [CrossRef]
39. Cibecchini, G.; Veronesi, M.; Catelani, T.; Bandiera, T.; Guarnieri, D.; Pompa, P.P. Antiangiogenic Effect of Graphene Oxide in Primary Human Endothelial Cells. *ACS Appl. Mater. Interfaces* **2020**, *12*, 22507–22518. [CrossRef]